Three-Dimensional Characterisation of Fibroblast Foci in Idiopathic Pulmonary Fibrosis

Mark G. Jones[1,2], Aurélie Fabre[3§], Philipp Schneider[4§], Francesco Cinetto[5], Giacomo Sgalla[1,2], Mark Mavrogordato[4], Sanjay Jogai[6], Aiman Alzetani[7], Ben G. Marshall[2], Katherine M.A. O'Reilly[8,9], Jane A. Warner[1], Peter M. Lackie[1], Donna E. Davies[1,2,10], David M. Hansell[11], Andrew G. Nicholson[12], Ian Sinclair[4], Kevin K Brown[13], Luca Richeldi[1,2,10]

[1]Academic Unit of Clinical and Experimental Sciences, Faculty of Medicine, University of Southampton, Southampton, UK; [2]National Institute for Health Research Respiratory Biomedical Research Unit, University Hospital Southampton, Southampton, UK; [3]Department of Histopathology, St. Vincent's University Hospital, Elm Park, Dublin, Ireland; [4]μ-VIS X-ray Imaging Centre, Faculty of Engineering and the Environment, University of Southampton, Southampton, UK; [5]Clinical Immunology, Department of Medicine, Padua University, Italy; [6]Department of Cellular Pathology, University Hospital Southampton, Southampton, UK; [7]Department of Cardiothoracic Surgery, University Hospital Southampton, Southampton, UK; [8]Mater Misericordiae University Hospital, Dublin, Ireland; [9]School of Medicine and Medical Science, University College Dublin, Dublin, Ireland; [10]Institute for Life Sciences, University of Southampton, Southampton, UK; [11]Department of Radiology, Royal Brompton Hospital and National Heart and Lung Institute, Imperial College, London, UK; [12]Histopathology Department, Royal Brompton Hospital and National Heart and Lung Institute, Imperial College, London, UK; [13]Department of Medicine, National Jewish Health, Denver, Colorado, USA

§These authors contributed equally to this work

Correspondence to:
Dr Mark Jones
Academic Unit of Clinical and Experimental Sciences
University of Southampton
Southampton General Hospital, Southampton, SO16 6YD
United Kingdom
Tel: +44 2381 203308 ; Fax: +44 23 80 511761; Email: Mark.Jones@soton.ac.uk

Declaration of interests

MM and IS have received grants from Nikon Metrology outside of the submitted work. AGN has received personal fees from Sanofi outside of the submitted work. KKB has received research support from NIH-NHLBI, and personal fees from Boehringer Ingelheim and National Jewish Health outside of the submitted work. DD has received personal fees from Synairgen outside of the submitted work. LR has received personal fees from Boehringer Ingelheim and Roche outside of the submitted work. All other authors declare that no conflict of interest exists.

ABSTRACT

In idiopathic pulmonary fibrosis (IPF), the fibroblast focus is a key histological feature representing active fibroproliferation. On standard 2D pathologic examination fibroblast foci are considered small, distinct lesions although they have been proposed to form a highly interconnected reticulum as the leading edge of a "wave" of fibrosis. Here, we characterised fibroblast focus morphology and inter-relationships in 3D using a novel integrated microCT and histological methodology. In 3D fibroblast foci were morphologically complex structures with large variations in shape and volume (range 1·3 x 10^4 to 9·9 x 10^7 μm^3). Within each tissue sample numerous multiform foci were present, ranging from a minimum of 0·9 to a maximum of 11·1 per mm^3 of lung tissue. Each focus was an independent structure and no interconnections were observed. Together, our data indicate that in 3D fibroblast foci form a constellation of heterogeneous structures with large variations in shape and volume, suggesting previously unrecognised plasticity. No evidence of interconnectivity is identified, consistent with the concept that foci represent discrete sites of lung injury and repair.

Word Count 176

INTRODUCTION

Idiopathic pulmonary fibrosis (IPF) is the prototypic fibrotic lung disease in which progressive scarring of the lungs leads to death by respiratory failure (1). The median survival of 3 years from diagnosis is worse than many cancers (2). Despite identification of activated fibroblasts as key effector cells pathologically remodelling the extracellular matrix, therapeutic options remain limited and a better understanding of disease pathogenesis is required (3-5).

Diagnosis of IPF is based on recognition of the usual interstitial pneumonia (UIP) pattern on chest high-resolution computed tomography (HRCT) or surgical lung biopsy (1). The histological pattern of UIP is believed to be produced by the consequences of repeated epithelial injury together with unfettered fibroproliferation (6). Aggregates of proliferating fibroblasts and myofibroblasts, termed "fibroblast foci", are a key histological diagnostic feature of UIP thought to represent areas of active fibrosis (7). On standard 2D pathologic examination fibroblast foci are considered small, distinct lesions and their profusion has been reported to be of prognostic significance, although study findings vary (8-12). They have been proposed to be linked in a complex reticulum that is highly interconnected and extends from the pleura into the underlying parenchyma (13), yet the 3D morphology and spatial inter-relationships of fibroblast foci remain poorly understood.

Micro-computed tomography (microCT) allows non-destructive imaging of tissue 3D microarchitecture down to spatial resolutions in the order of 1-10 μm (14, 15). It has informed our understanding of distal airways disease in patients with end-stage chronic obstructive pulmonary disease (COPD) and chronic lung allograft rejection (16, 17). In fibrotic lung diseases microCT imaging has been employed for quantification of fibrosis in small animal studies (18-23), however as samples have required processing with contrast agents or air-inflation prior to fixation, application to diagnostic human interstitial lung disease tissue

samples has not been possible with tissue access extremely limited. We have recently developed a protocol that allows imaging of routinely prepared formalin-fixed paraffin-embedded human lung tissue samples by microCT (24). This non-destructive process can be applied to tissue used for diagnosis, and conventional histopathologic sectioning of the tissue can subsequently be performed; this enables cellular or molecular information from methodologies such as immunohistochemistry or *in situ* hybridisation to be precisely co-registered within the volumetric data set from microCT.

Given the pivotal nature of fibroproliferation to the progression of IPF and the key role that fibroblast foci are believed to play in this process (6), new insights into the structure of these lesions may further advance our understanding of whether they are inter-linked in a complex reticulum as the leading edge of a "wave" of fibrosis or they comprise multiple distinct structures that have arisen as a consequence of multi-focal lung injury (6, 13). In our study we applied a novel integrated microCT and histological methodology on formalin-fixed paraffin-embedded diagnostic lung tissue to study the morphology of fibroblast foci in 3D. Our work demonstrates the potential for 3D imaging methodologies to further inform concepts of the underlying pathogenesis of fibrotic lung diseases and reveals that, in contrast to current understanding from standard pathology of 2D tissue sections, in 3D fibroblast foci form a constellation of heterogeneous structures with large variations in shape and volume, suggesting previously unrecognised plasticity. We identify no evidence of general interconnectivity, consistent with the concept that foci represent discrete sites of lung injury and repair.

RESULTS

MicroCT of formalin-fixed paraffin-embedded lung tissue identifies diagnostic features of the UIP pattern. Firstly, we assessed visualisation of diagnostic paraffin-embedded lung tissue 3D microarchitecture by microCT. MicroCT enabled interactive multi-planar assessment of tissue microarchitecture (Video 1, available for download online). 3D reconstructions identified clear morphological differences between normal and IPF lung tissue, with volume renderings in Figure 1 demonstrating loss of alveolar structures and increased parenchymal thickness in IPF, consistent with previous stereological findings (25). Videos 2 and 3 visualise rotation of these volume renderings. Feature correspondence between corresponding histological sections and microCT slices of IPF lung tissue was assessed, with qualitative comparison (Figure 2) demonstrating that microCT can visualise normal lung structural features such as airways, blood vessels, and alveolar airspaces, in addition to structural features of the UIP pattern, including heterogeneity of the distribution of interstitial fibrosis and normal appearing lung, architectural distortion, and honeycomb change.

Fibroblast foci are locally complex, hetereogeneous structures in 3D. We then studied whether fibroblast foci were identifiable in microCT image data. Correlation of histological slices and co-registered microCT images established features which typically enabled identification of fibroblast foci greater than 200 μm when integrated with visualisation in three different planes (*xy*, *xz*, *yz*), specifically when the foci were adjacent to airspaces, given their reduced greyscale intensity when compared to surrounding tissue as illustrated in Figure 3 and Supplementary Appendix Figure S1.

Initial visual 3-plane microCT analyses suggested a locally complex fibroblast focus morphology in 3D that was not apparent on cross-sectional 2D histopathologic examination. To confirm this finding we performed histological identification of fibroblast foci followed by segmentation of the corresponding image sections within the microCT volume to enable

accurate integrated assessment of their 3D structure. Fibroblast foci were digitally labelled in the corresponding microCT slice every 8 μm over 1000 μm, using the segmentation editor, having been identified in the histological sections as aggregates of spindle-shaped cells with a characteristic blue-green colour on Movat's pentachrome stain or pale colour on haematoxylin and eosin stain, representing focal deposits of young, immature collagen and proteoglycans within the sub-epithelial interstitium. All foci within the microCT field of view were labelled. 3D visualisation and quantification of the segmented data identified complex discrete structures with marked variation in size and shape (Figure 4, Supplementary Appendix Figure S2, Table 1, and Video 4) that appear to be a non-uniform process. The 3D render visualised in Figure 4 is available for download online (Supplementary Render 1).

Fibroblast focus volumes ranged from $1{\cdot}6 \times 10^4$ to $9{\cdot}9 \times 10^7$ μm^3. No evidence of substantial extension of individual foci inwards from the pleura to the parenchyma was identified. Review of digitally imaged sequential 2D histology sections identified the complex morphology of an individual fibroblast focus in 3D, with a number of apparently independent fibroblast foci in 2D identified to form one morphologically discrete structure. These foci ranged from relatively simple 3D structures (Supplementary Figure S3) to more morphologically complex structures adjacent to established fibrosis (Figure 5).

Fibroblast foci are not generally interconnected. MicroCT 3-plane visualisation, 3D segmentations (Figure 6 and Video 5), and sequential 2D histology section review were evaluated for evidence of fibroblast focus interconnectivity at a larger scale, with numerous independent multiform fibroblast structures identified in each tissue volume and fibroblast focus frequency ranging from 0·9 to 11·1 per mm^3 of lung tissue. The Euler number, a measure of redundancy in a network, was calculated for each case and identified no evidence of fibroblast focus interconnectivity (see Table S1 in the Supplementary Appendix) (26, 27).

Given the identified variability of foci in 3D, fibroblast focus profusion on 2D histological sections was then semi-quantitatively and quantitatively assessed over a depth of 1 mm of lung tissue from each patient. Analyses identified variability both quantitatively (up to 4-fold intra-tissue variation) and semi-quantitatively (Supplementary Appendix Figure S4). An exploratory analysis investigating the association between 3D fibroblast focus density and change in forced vital capacity (FVC) over 1 year identified a negative correlation (Supplementary Appendix Figure S5).

DISCUSSION

Through a novel integrated histological and microCT analysis of IPF lung tissue we characterised fibroblast foci in 3D, identifying that they are morphologically complex structures with large variations in shape and volume. Within each tissue sample, numerous discrete fibroblast structures were present, without evidence of general interconnectivity.

Whilst IPF remains an idiopathic disease there have been several proposals regarding mechanisms of pathogenesis, one of which is that fibroblast foci form a highly complex and interconnected reticulum extending from the pleura to the lung parenchyma as a "wave" of progressive fibroproliferation (13, 28, 29). This concept was informed by a study from Cool *et al* in which a computer-generated 3D reconstruction and Euler connectivity analysis of histological sections over a depth of 500 μm were proposed to demonstrate an interconnected fibroblast reticulum (13). However, the methodological advances of our work enabled analysis of far larger tissue volumes than previously possible, and we identify that the preceding reconstruction scale was consistent with visualisation of one fibroblast focus of comparable dimensions to that shown in Figure 4. With multiple methodologies our analyses show that fibroblast foci are independent discrete structures, and as a group, are not part of a reticulum. In support of this finding, human androgen receptor gene methylation assay analysis of foci by Cool *et al* identified balanced methylation indicating polyclonality of foci (13). Our results are consistent with the concept that fibroblast foci represent discrete non-connected sites of localised lung injury, with 3D reconstructions identifying a constellation of independent fibroblast structures in support of the paradigm that IPF is a consequence of aberrant wound healing responses to local micro-injuries (6).

At a 2D cross-sectional histological level, fibroblast foci are usually considered small, distinct lesions (7, 30), although they are often found grouped in proximity, forming what are thought to be areas of active fibrosis. Our results show that in 3D, foci in proximity and

typically with shared areas of established fibrosis form one complex discrete fibroblast structure. A heterogeneous population is identified with large variations in size and shape, and over a 100-fold difference between largest and smallest volume fibroblast foci. Acknowledging that the cause of lung injury in IPF has yet to be determined we speculate on a number of possibilities for this finding, which suggests previously unrecognised plasticity. It is possible that the size and morphology of an individual focus reflects the extent and distribution of injury at a lung surface. Alternatively, volume variation could indicate temporal growth of foci, with the smallest foci occurring at the most recent sites of injury. The latter possibility is in keeping with our identification of small isolated foci. Further work would be required to investigate these relationships in more detail.

Whilst increased profusion of fibroblast foci has been proposed to correlate with mortality in patients with IPF, a number of studies have identified no association, and the clinical significance of this finding remains uncertain (8-12). Differences in patient selection and methodology have been suggested to account for discordant findings, with marked variations in methodologies including semi-quantitative scoring, quantitative point-counting of random fields or whole slide fibroblast focus quantification. No previous study has systematically assessed variability of foci within tissue samples. Our data identify fibroblast focus profusion can vary markedly over a 1mm depth of tissue, however, studies correlating profusion with mortality have typically reviewed one or two tissue sections per lobe sampled. Focus variability within tissue samples should therefore be considered in future studies correlating fibroblast focus profusion with clinical outcome. In support of the concept of fibroblast foci as a marker of disease activity was our finding of a possible association between 3D fibroblast focus density and FVC change. However, given our limited sample size larger studies would be required to confirm such an association.

Although significant progress has been made, our understanding of the pathogenesis and treatment of IPF remains limited (6). Nintedanib and pirfenidone are two novel anti-fibrotic drugs that were recently shown to approximately halve the rate of decline of lung function in IPF (4, 5), with both having multiple actions on the proliferation and signalling pathways of fibroblasts and myofibroblasts (31-34). Additional therapies are urgently required since these two drugs only reduce the rate of disease progression. This study emphasises the importance of investigating new agents which prevent and/or ameliorate the repeated lung injuries that result in multi-focal sites of fibroproliferation.

Initial work correlated microCT of whole paraffin-embedded samples of UIP tissue with histological sections. Whilst soft tissue visualisation through conventional X-ray-based CT is a challenge due to the low X-ray absorption of soft tissues, our microCT imaging protocol was optimised to provide the necessary image contrast between soft tissue and paraffin, and also between different micro-architectural features within the tissue itself (24). Excellent micro-architectural feature correlation between histology and microCT imaging was observed, and diagnostic structural features of a pattern of UIP were visualised. Whereas larger fibroblast foci were directly visible within microCT image data, typically those less than 200μm were not. In the future, identification and segmentation of smaller fibroblast foci may be possible through improved contrast resolution, thresholding and pattern recognition approaches. Automated approaches, based on exploiting the X-ray attenuation contrast window between tissue and paraffin mounting medium, and also between different tissue compartments may further facilitate subsequent visualisation and quantification.

There are significant advantages to the use of paraffin-embedded tissue to study fibrotic interstitial lung diseases. Whilst images of paraffin-embedded tissue have a lower contrast than air-inflated, fixed and dried tissue samples, access to sufficient fresh or frozen diagnostic tissue with robust histopathological integration poses significant challenges in

fibrotic ILDs. The availability of large banks of archived diagnostic paraffin-embedded samples facilitates systematic microCT analyses of fibrotic ILDs. Similarities and differences may further advance our understanding of underlying pathophysiology and potentially inform stratification approaches in fibrotic lung diseases. Given the diagnostic challenges that ILD histopathology poses, the ability to visualize in 3D could ultimately have diagnostic application. Furthermore, use of paraffin-embedded samples allows integration of co-registered histology sections within the 3D microCT volumetric data set; this enables accurate 3D analyses of the relationship of cellular and micro-architectural features of fibrotic lung diseases. Whilst a predominantly manual segmentation methodology was applied during this initial study, development of automatic and semi-automatic methodologies will further enable quantitative feature extraction and analyses such as 3D topographical distribution of lung fibrosis.

Our study has demonstrated that the application of novel 3D imaging methodologies can further advance concepts of disease pathogenesis in fibrotic lung diseases. It has identified that fibroblast foci are heterogeneous and of varying size, complexity and frequency in each patient's biopsy, suggesting previously unrecognised plasticity. We have also shown that these fibroblast structures are independent of each other, consistent with their being the product of discrete sites of lung injury and repair.

METHODS

Clinical material. Clinically indicated diagnostic surgical lung biopsy specimens from four patients (see Table 2 for further clinical details) with a subsequent multidisciplinary diagnosis of IPF according to international consensus guidelines were studied (1). No patient had clinical or radiological evidence of an acute exacerbation prior to or at time of biopsy. Specimens had been diagnosed as showing a typical UIP pattern, confirmed by the independent review of two expert pulmonary pathologists, the samples having received standard processing with fixation in neutral buffered formalin for 48 hours and embedding in paraffin wax. Control formalin-fixed paraffin-embedded healthy lung tissue was from macroscopically normal lung sampled remote from the cancer site in two patients undergoing surgery for lung cancer.

MicroCT imaging protocol. The paraffin-embedded lung samples were scanned using a custom-built Nikon Metrology microCT scanner at an isotropic voxel size of 8 μm as previously described (24), with optimisation to maximise soft tissue contrast. An X-ray tube potential peak of 55 kVp was used at a beam current of 104-114 μA. 2601 tomographic radiographic viewpoints of the samples were assessed (360° rotation in 0.14° steps) by acquiring 64 repeated projections (2000x2000 pixels) for each angular step to increase signal-to-noise ratio through frame averaging, where integration time for individual projections was set to 500 ms at an isotropic voxel size of 8 μm, resulting in a field of view of 16x16 mm^2. Together with sample shuttling during acquisition to suppress ring artefacts with the reconstruction, the gross image acquisition time per sample was about 24 hours. The projections were then reconstructed in 3D using the Feldkamp, Davis, and Kress algorithm for cone beam tomography in the DigiR3D tomography reconstruction module of the DigiXCT software suite (Digisens, Le Bourget-du-Lac, France) or using standard filtered-

back projection within CTPro3D (v. XT 2·.2 service pack 10, Nikon Metrology, UK) and CTAgent (v. XT 2·2 service pack 10, Nikon Metrology, UK) (35).

Histology acquisition. Following microCT imaging 4 μm-thick serial sections were cut over an approximate depth of 1000 μm. Sections every 8 μm (corresponding to the actual microCT voxel size of 8 μm) were de-paraffinised and stained using modified Movat's pentachrome or hematoxylin and eosin stain (36). Whole sections were imaged using a 20· objective on a Dot-Slide scanning system (Olympus, Southend-on-Sea, UK), and visualised with Olyvia 2·6 (Olympus, Southend-on-Sea, UK).

MicroCT image visualization and correlation with histological sections. Image pre-processing, segmentation, 3D volume reconstruction, and quantification of lung sample microCT data were performed with AvizoFire 7·1 (FEI, Oregon, USA). Three or more structural features in each microCT volume were matched to a specific histological section, and the 3D orientation of the microCT volume was correspondingly transformed for plane correspondence between histological and microCT data. For direct comparisons of histological and microCT sections the Fiji distribution of ImageJ (version 1·49p) plugin Landmark Correspondences was used to co-register the images after the initial matching for plane correspondence (37, 38).

MicroCT segmentation and analyses. Fibroblast foci were digitally labelled in the corresponding microCT slice every 8 μm over 1000 μm, using the segmentation editor, having been identified in the histological sections as aggregates of spindle-shaped cells with a characteristic blue-green colour on Movat's pentachrome stain or pale colour on haematoxylin and eosin stain, representing focal deposits of young, immature collagen and proteoglycans within the sub-epithelial interstitium. The contours of fibroblast foci within corresponding microCT slices were drawn using the 'Lasso' function in AvizoFire. All foci within the microCT field of view were labelled. Missing levels (for example due to ribbon

section breaks) were manually interpolated. Following tissue segmentation individual foci were then tagged by the labelling function, and individual foci were considered as separate structures if they had no common voxel faces, edges, or corners. The foci were then visualised through volume rendering using a cyclic colour map so that foci in close proximity were more likely to be shown in a different colour. Volume, 3D shape, and occurrence were quantified. For 3D volume renderings and calculation of lung tissue volume, paraffin was segmented from each microCT volumetric data set. Global thresholding followed by the 'Smooth Labels' function was applied, with the threshold identified as the mean greyscale value of a 1 mm^3 volume of paraffin. An example of these steps is shown in Supplementary Figure S6. Using the 'Crop' function the subvolume corresponding to the histological stack was then extracted, and lung tissue volume quantified.

Fibroblast focus quantitation and connectivity analyses. Connectivity between fibroblast foci was assessed visually through microCT 3-plane visualisation, 3D foci segmentations, and corresponding sequential 2D histology section review. Total number of foci per case and fibroblast foci tissue density were calculated. Stereological analysis was performed and fibroblast foci every 20–30 μm over approximately 1000 μm were marked on photo-micrographed whole tissue sections using Olyvia. Fibroblast focus profusion was semi-quantitatively (scale 0 – 6) or quantitatively (fibroblast foci per cm^2 of tissue) measured on these sections. The Euler-Poincaré characteristic or Euler number (27, 39), a measure of redundancy in a network, was calculated. Full details are provided in the Methods section of the Supplementary Appendix.

Statistics. All graphs were created using GraphPad Prism software, and statistical analyses were calculated using GraphPad Prism (version 6; GraphPad Software). The correlation between one year FVC percentage change and fibroblast focus density was determined by linear regression. A *P* value of less than 0.05 was considered significant.

Study approval. The study was approved by the local Research Ethics Committee (Ref 07/H0607/73), and all subjects gave written informed consent.

Author Contributions

M.G.J., A.F., P.S., D.D., and L.R. conceived the project, designed experiments, analysed data, and wrote the manuscript. P.M.L., J.A.W., K.M.A.O., and I.S. contributed to the project conception, planning and experimental design. M.G.J., A.F., G.S., F.C., M.M., and S.J. performed experiments and analysed data. A.A., B.G.M., and K.M.A.O contributed to clinical sample collection. K.K.B. contributed to data interpretation, data review, and manuscript revision. D.M.H. and A.G.N. contributed to the conception and design of the study and reviewed data. All authors reviewed, revised, and approved the manuscript for submission.

Acknowledgments

This study was supported by a Wellcome Trust Clinical Research Training Fellowship (100638/Z/12/Z; to MGJ). Infrastructure support was funded by the NIHR Southampton Respiratory Biomedical Research Unit. EPSRC grant EP-H01506X is acknowledged for provision of the μ-VIS X-ray Imaging facilities. AGN and DMH were supported by the National Institute of Health Research Respiratory Disease Biomedical Research Unit at the Royal Brompton and Harefield NHS Foundation Trust and Imperial College London. We thank the staff of the NIHR Wellcome Trust Southampton Clinical Research Facility, the Biomedical Imaging Unit, the Histochemistry Research Unit, and the μ-VIS computed tomography centre at the University of Southampton.

REFERENCES

1. Raghu G, et al. An Official ATS/ERS/JRS/ALAT Statement: Idiopathic Pulmonary Fibrosis: Evidence-based Guidelines for Diagnosis and Management. *Am J Respir Crit Care Med.* 2011;183(6):788–824.

2. Meltzer EB, Noble PW. Idiopathic pulmonary fibrosis. *Orphanet J Rare Dis.* 2008;3(1):8.

3. Noble PW, Barkauskas CE, Jiang D. Pulmonary fibrosis: patterns and perpetrators. *J Clin Inves.t* 2012;122(8):2756–2762.

4. King TE Jr., et al. A Phase 3 Trial of Pirfenidone in Patients with Idiopathic Pulmonary Fibrosis. *N Engl J Med.* 2014;370(22):2083–2092.

5. Richeldi L, et al. Efficacy and Safety of Nintedanib in Idiopathic Pulmonary Fibrosis. *N Engl J Med.* 2014;370(22):2071–2082.

6. King TE, Pardo A, Selman M. Idiopathic pulmonary fibrosis. *Lancet.* 2011;378(9807):1949–1961.

7. Katzenstein AL, Myers JL. Idiopathic pulmonary fibrosis: clinical relevance of pathologic classification. *Am J Respir Crit Care Med.* 1998;157(4):1301–1315.

8. King TE Jr, et al. Idiopathic pulmonary fibrosis - Relationship between histopathologic features and mortality. *Am J Respir Crit Care Med.* 2001;164(6):1025–1032.

9. Nicholson AG, et al. The relationship between individual histologic features and disease progression in idiopathic pulmonary fibrosis. *Am J Respir Crit Care Med.* 2002;166(2):173–177.

10. Harada T, Watanabe K, Nabeshima K, Hamasaki M, Iwasaki H. Prognostic significance

of fibroblastic foci in usual interstitial pneumonia and non-specific interstitial pneumonia. *Respirology* 2013;18(2):278–283.

11. Flaherty KR, et al. Fibroblastic Foci in Usual Interstitial Pneumonia. *Am J Respir Crit Care Med.* 2003;167(10):1410–1415.

12. Hanak V, et al. Profusion of fibroblast foci in patients with idiopathic pulmonary fibrosis does not predict outcome. *Respir Med.* 2008;102(6):852–856.

13. Cool CD, et al. Fibroblast Foci Are Not Discrete Sites of Lung Injury or Repair: The Fibroblast Reticulum. *Am J Respir Crit Care Med.* 2006;174(6):654–658.

14. Paulus MJ, Gleason SS, Kennel SJ, Hunsicker PR, Johnson DK. High resolution X-ray computed tomography: An emerging tool for small animal cancer research. *Neoplasia.* 2000;2(1-2):62–70.

15. Metscher BD. MicroCT for developmental biology: A versatile tool for high-contrast 3D imaging at histological resolutions. *Dev Dyn.* 2009;238(3):632–640.

16. McDonough JE, et al. Small-airway obstruction and emphysema in chronic obstructive pulmonary disease. *N Engl J Med.* 2011;365(17):1567–1575.

17. Verleden SE, et al. The Site and Nature of Airway Obstruction after Lung Transplantation. *Am J Respir Crit Care Med.* 2014;189(3):292–300.

18. Scotton CJ, et al. Ex vivo micro-computed tomography analysis of bleomycin-induced lung fibrosis for preclinical drug evaluation. *Eur Resp J.* 2013;42(6):1633–1645.

19. Ask K, et al. Comparison between conventional and “clinical” assessment of experimental lung fibrosis. *J Transl Med.* 2008;6(1):16.

20. Rodt T, et al. Micro-computed tomography of pulmonary fibrosis in mice induced by adenoviral gene transfer of biologically active transforming growth factor-b1. *Respir Res.* 2010;11(1):181.

21. Cavanaugh D, et al. Quantification of bleomycin-induced murine lung damage in vivo with micro-computed tomography. *Acad Radiol.* 2006;13(12):1505–1512.

22. De Langhe E, et al. Quantification of Lung Fibrosis and Emphysema in Mice Using Automated Micro-Computed Tomography. *PLoS ONE.* 2012;7(8):e43123.

23. Shofer S, Badea C, Auerbach S, Schwartz DA, Johnson GA. A MicroCT-Based Method for the Measurement of Pulmonary Compliance in Healthy and Bleomycin-Exposed Mice. *Exp Lung Res.* 2007;33(3-4):169–183.

24. Scott AE, et al. Three Dimensional Imaging of Paraffin Embedded Human Lung Tissue Samples by Micro-Computed Tomography. *PLoS ONE* 2015;10(6):e0126230.

25. Coxson HO, et al. Quantification of idiopathic pulmonary fibrosis using computed tomography and histology. *Am J Respir Crit Care Med.* 1997;155(5):1649–1656.

26. Ochs M, et al. The Number of Alveoli in the Human Lung. *Am J Respir Crit Care Med.* 2004;169(1):120–124.

27. Gundersen HJ, et al. The New Stereological Tools - Disector, Fractionator, Nucleator and Point Sampled Intercepts and Their Use in Pathological Research and Diagnosis. *APMIS.* 1988;96(10):857–881.

28. Vancheri C, Failla M, Crimi N, Raghu G. Idiopathic pulmonary fibrosis: a disease with similarities and links to cancer biology. *Eur Resp J.* 2010;35(3):496–504.

29. Leslie KO. Idiopathic pulmonary fibrosis may be a disease of recurrent, tractional injury to the periphery of the aging lung: a unifying hypothesis regarding etiology and pathogenesis. *Arch Pathol Lab Med.* 2012;136(6):591–600.

30. Katzenstein AL, Myers JL, Prophet WD, Corley LS, Shin MS. Bronchiolitis obliterans and usual interstitial pneumonia. A comparative clinicopathologic study. *Am J Surg Pathol.* 1986;10(6):373–381.

31. Conte E, et al. Effect of pirfenidone on proliferation, TGF-β-induced myofibroblast differentiation and fibrogenic activity of primary human lung fibroblasts. *Eur J Pharm Sci.* 2014;58:13–19.

32. Iyer SN, Gurujeyalakshmi G, Giri SN. Effects of pirfenidone on procollagen gene expression at the transcriptional level in bleomycin hamster model of lung fibrosis. *J Pharmacol Exp Ther.* 1999;289(1):211–218.

33. Rangarajan S, et al. Novel Mechanisms for the Anti-Fibrotic Action of Nintedanib. *Am J Respir Cell Mol Biol.* 2016;54(1):51-59.

34. Wollin L, Maillet I, Quesniaux V, Holweg A, Ryffel B. Anti-fibrotic and anti-inflammatory activity of the tyrosine kinase inhibitor, nintedanib, in experimental models of lung fibrosis. *J Pharmacol Exp Ther.* 2014;349:209–220.

35. Feldkamp LA, Davis LC, Kress JW. Practical Cone-Beam Algorithm. *J Opt Soc Am A Opt Image Sci Vis.* 1984;1(6):612–619.

36. Russell HK. A modification of Movat's pentachrome stain. *Arch Pathol Lab Me.d* 1972;94(2):187–191.

37. Schindelin J, et al. Fiji: an open-source platform for biological-image analysis. *Nat Meth.*

2012;9(7):676–682.

38. Saalfeld S, Cardona A, Hartenstein V, Tomancak P. As-rigid-as-possible mosaicking and serial section registration of large ssTEM datasets. *Bioinformatics.* 2010;26(12):i57–i63.

39. Nyengaard JR, Marcussen N. The number of glomerular capillaries estimated by an unbiased and efficient stereological method. *J Microsc.* 1993;171(Pt 1):27–37.

FIGURES

Figure 1. 3D volume renderings of normal and UIP/IPF lung tissue imaged by microCT. Cubes (2 mm per side) of (A) normal lung tissue and (B) usual interstitial pneumonia (UIP) / idiopathic pulmonary fibrosis (IPF) lung tissue were digitally extracted from the reconstructed microCT lung tissue volumes following removal of paraffin by absolute thresholding. For reference on the superior surface a co-registered histological section stained with Movat's Pentachrome-stain is displayed. Morphological differences in 3D are apparent with UIP/IPF tissue demonstrating loss of alveolar structures and increased parenchymal thickness with an impression of "fullness" within the UIP/IPF tissue.

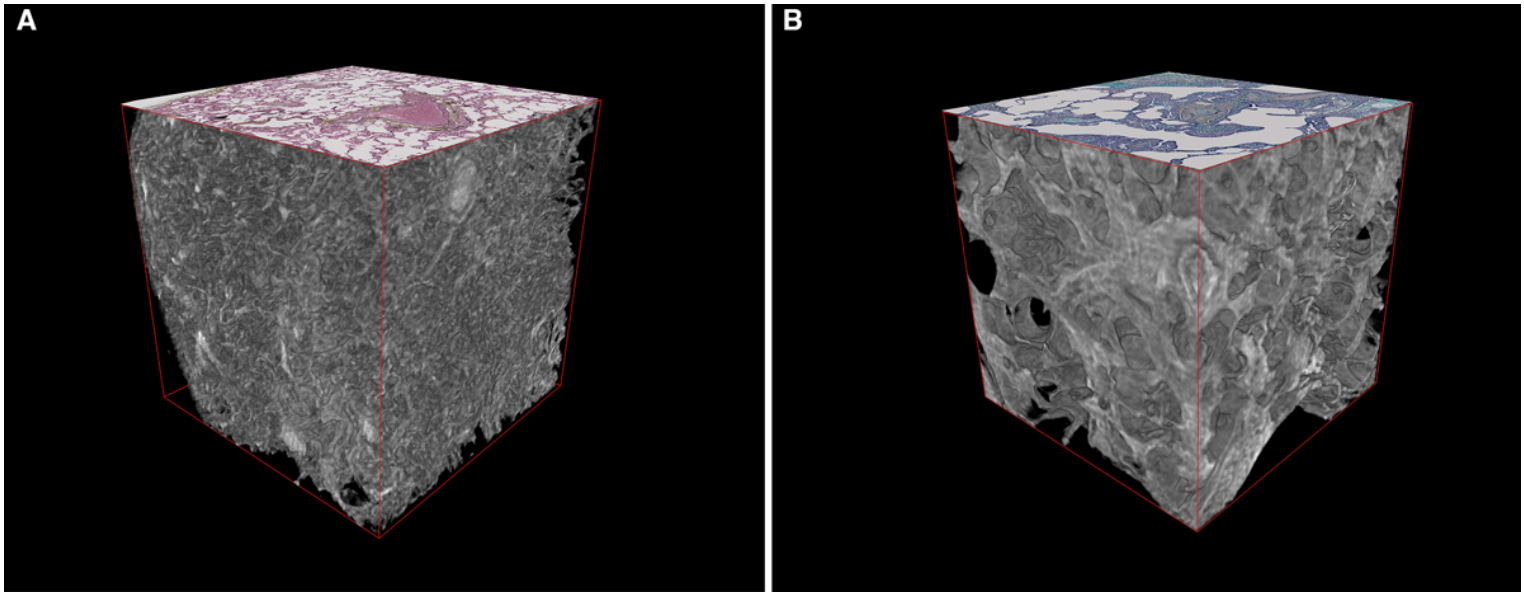

Figure 2. Correspondence of structural details identified by microCT to those seen by light microscopy. Registration based image matching of a histological section of usual interstitial pneumonia / idiopathic pulmonary fibrosis tissue (A, C) stained with Movat's Pentachrome-stain and corresponding microCT images (B, D). (C) and (D) are sub-areas of (A) and (B). Scale bar in (D) is 500 µm.

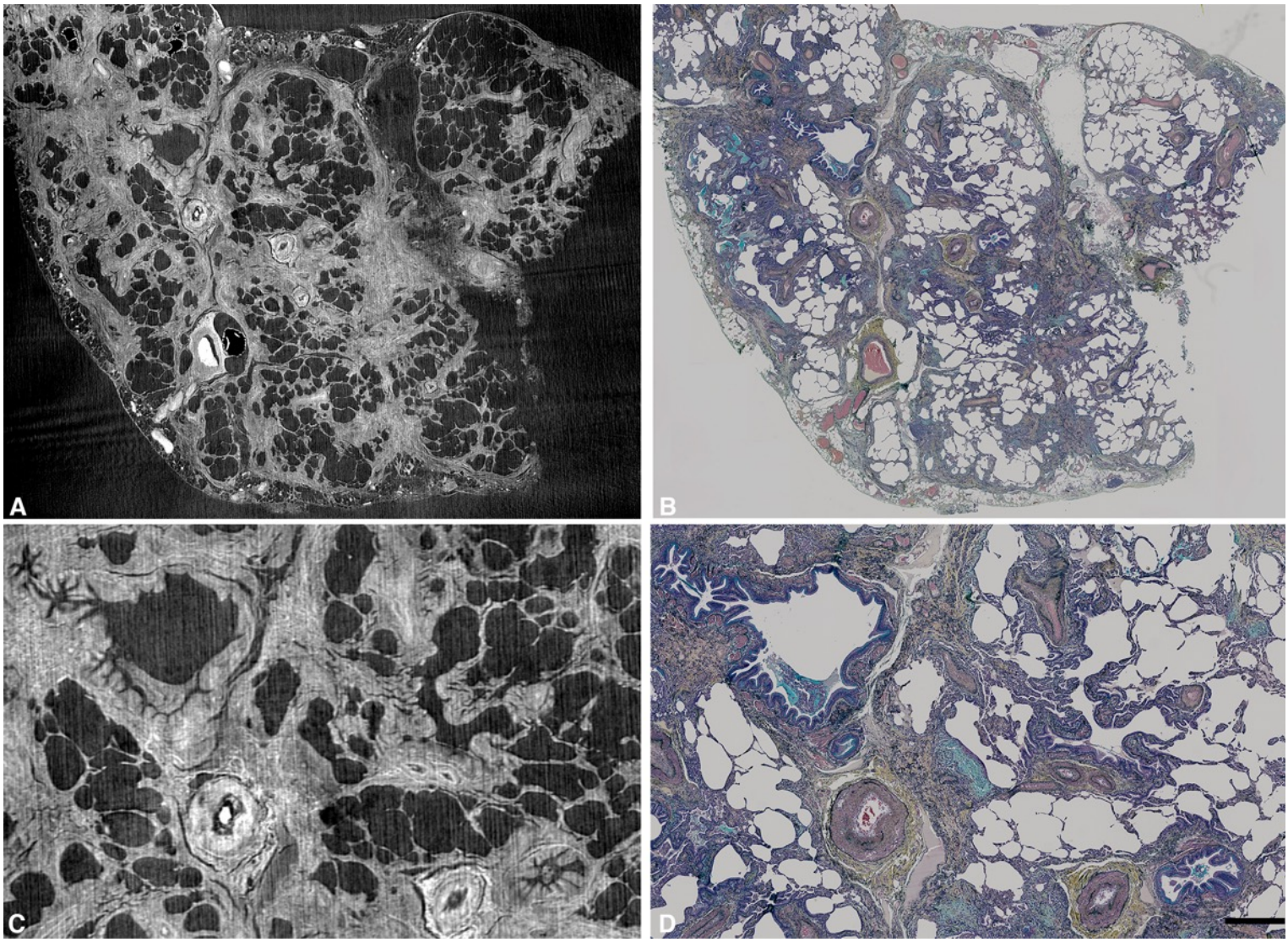

Figure 3. Multi-plane visualisation of a fibroblast focus with microCT. (A) Movat's Pentachrome stain of usual interstitial pneumonia / idiopathic pulmonary fibrosis tissue with a fibroblast focus identified by the *. The corresponding area of the microCT volume is seen in the *xy*-plane in (B), but in addition, the focus can also be visualised in the *xz*-plane (C) and in the *yz*-plane (D), enabling further assessment of the 3D morphology of fibroblast foci. Scale bar in (A) is 200 µm.

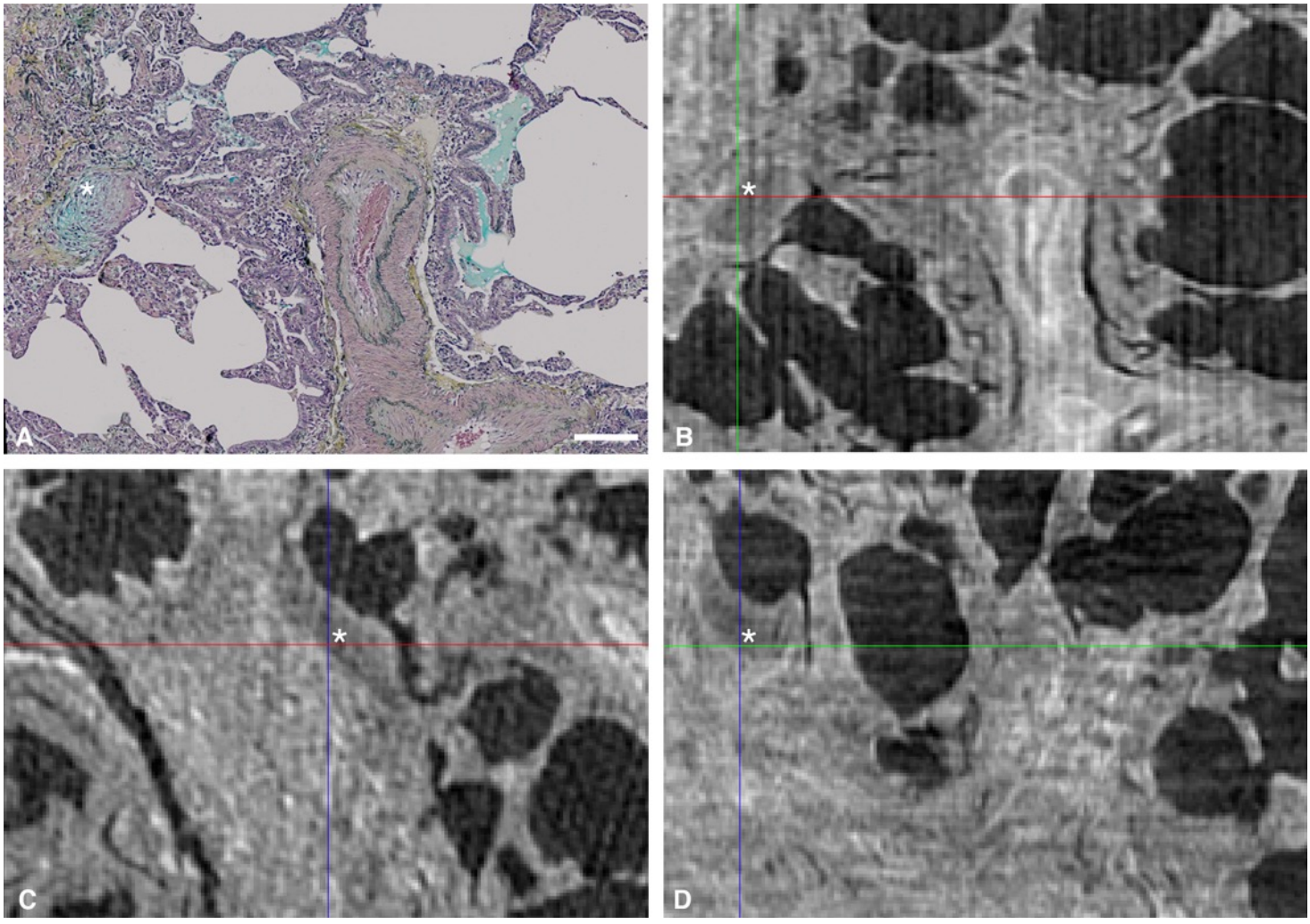

Figure 4. Fibroblast foci are locally complex structures. A computer generated 3D surface view rendering of one fibroblast focus from microCT segmentation identifies that fibroblast foci are locally complex structures in 3D. The focus is blue and for reference the pleural surface is visualised in yellow (height 1 mm) with a microCT slice inferiorly.

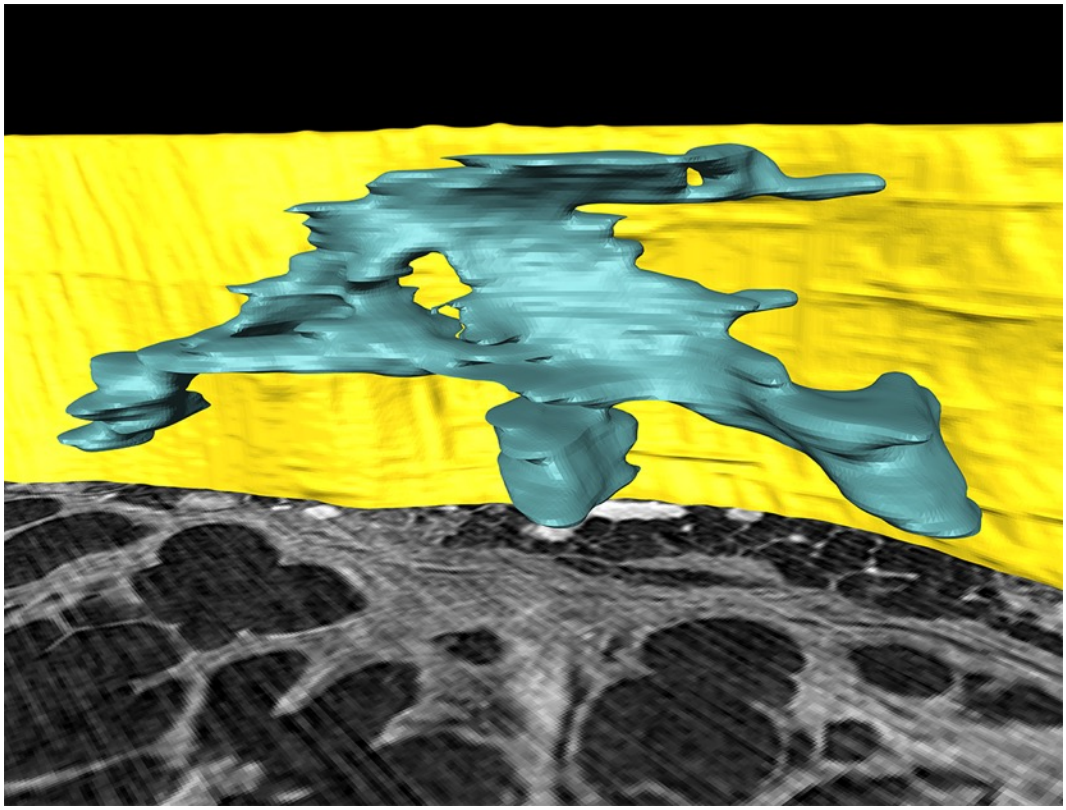

Figure 5. Review of co-aligned Movat's pentachrome-stained sections of an area of usual interstitial pneumonia tissue demonstrates the complex morphology of one fibroblast focus in 3D. Following identification of one fibroblast focus (A, black arrow), illustrative photomicrographs (A-M) demonstrate the changes in morphology of one fibroblast structure when sequential sections are visually reviewed, with apparently discrete foci forming part of one locally complex individual structure in 3D. In (N) and (O) the focus is no longer visible. Section depth in microns is indicated for each photomicrograph. Scale bar in (A) is 500 µm. The 3D rendering of this fibroblast focus is visualised in Figure 4 and Supplementary Video 4.

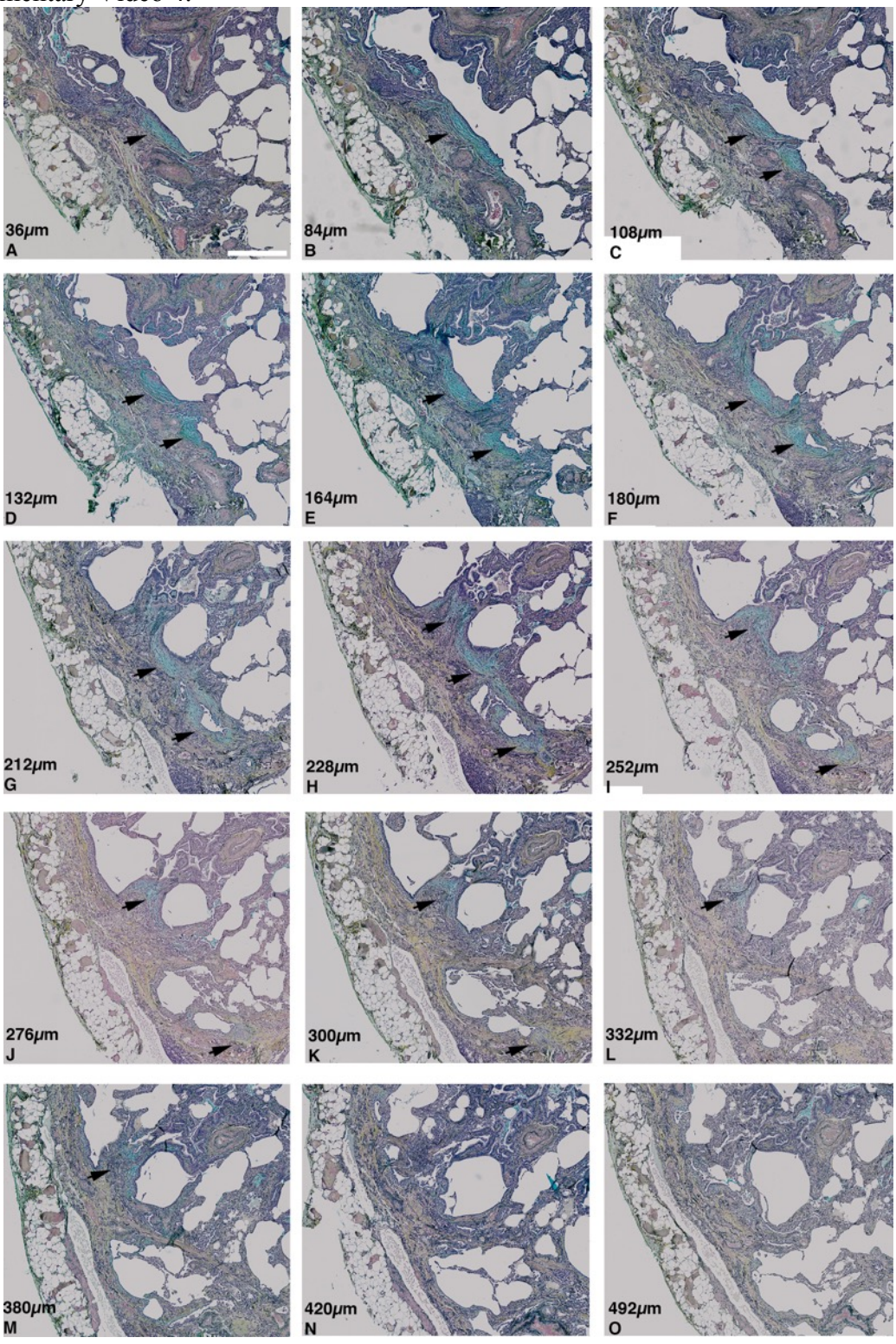

Figure 6. Fibroblast foci are discrete structures in 3D. Computer-generated 3D surface view renderings of all fibroblast foci from two microCT segmentations. Case 2 (A and C) has the lowest number density of fibroblast foci per mm^3 of lung tissue. Case 3 (B and D) has the highest number density. In (A) and (B) a 3D surface view rendering is shown in the *xy* plane (corresponding to the histological sectioning plane) with tissue boundaries marked by the dashed grey lines. In (C) and (D) a 3D surface view rendering is shown with a corresponding microCT slice displayed inferiorly (depth 1 mm). Scale bar is 2 mm.

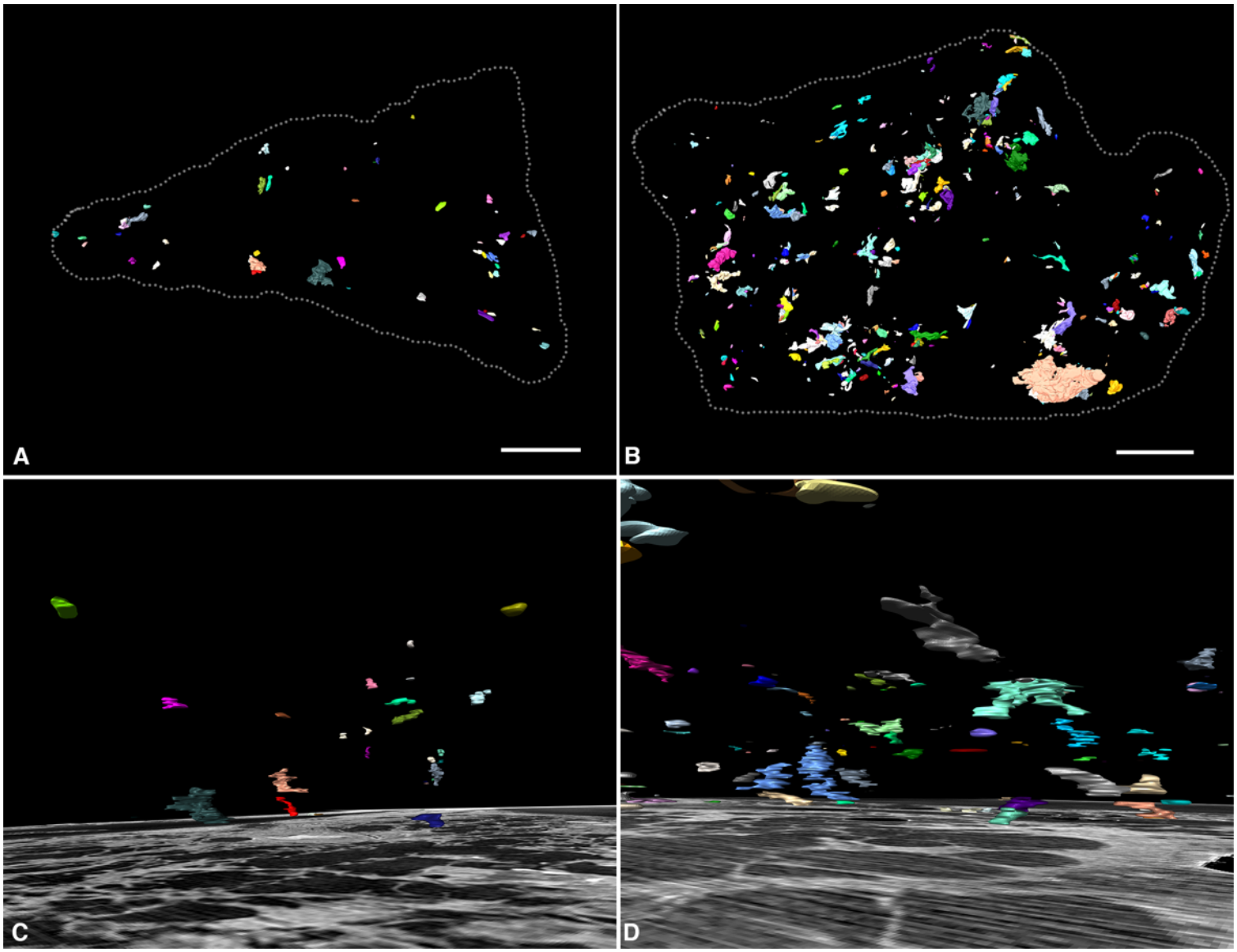

Table 1. Fibroblast focus measurements. For each microCT volumetric data set (n=4) lung tissue was segmented from paraffin through global thresholding with the threshold fixed at the mean greyscale value of a 1 mm^3 volume of paraffin. The sub-volume (256 mm^3) of the microCT data corresponding to the histological stack was extracted and the tissue volume quantified. Fibroblast foci were digitally labelled within the microCT volume, and volume, surface area, and density quantified.

Case	Tissue volume (mm^3)	Total number of fibroblast foci	Mean fibroblast focus volume (μm^3)	Mean fibroblast focus surface area (μm^2)	Number of fibroblast foci per mm^3 of lung tissue
1	55.11	219	1259719 ± 428674	151707 ± 49574	4·0
2	58.77	52	1512851 ± 532603	131315 ± 34518	0·9
3	50.0	553	1269145 ± 214309	142599 ± 21073	11·1
4	24.75	124	1394336 ± 354353	128756 ± 29022	5·0

* Values are mean ± SEM

Table 2. Patient demographics and longitudinal clinical data for the 4 subjects with usual interstitial pneumonia (UIP) / idiopathic pulmonary fibrosis (IPF).

Case	Gender	Age at biopsy	FVC % predicted within 3 months of biopsy	Absolute FVC % change 1yr post biopsy	Vital status
1	F	61	81	-4	Alive at 42 months follow up
2	M	66	63	-3	Alive at 24 months follow up
3	F	74	86	-23	Died 41 months post biopsy
4	M	72	81	-7	Died 18 months post biopsy

FVC: Forced vital capacity